

**Supporting Information for Evaluating the Effect of Ionic Strength on PNA:DNA Duplex
Formation Kinetics**

Colin S. Swenson¹, Hershel H. Lackey², Eric J. Reese², Joel M. Harris², Jennifer M. Heemstra¹,
Eric M. Peterson²

¹Department of Chemistry, Emory University, Atlanta, GA 30322

²Department of Chemistry, University of Utah, Salt Lake City, UT 84112

Table of Contents:

TABLE S1	S2
SINGLE MOLECULE IMAGING DATA ANALYSIS	S3
FIGURE S1	S3
FIGURE S2	S4
FIGURE S3	S5
FIGURE S4	S6
FIGURE S5	S7
FIGURE S6	S8
FIGURE S7	S9
VAN'T HOFF ANALYSIS OF PNA:DNA DUPLEX FORMATION	S10
TRANSITION STATE ENERGIES OF DUPLEX FORMATION	S10
TABLE S2	S12
TABLE S3	S12
TABLE S4	S13
TABLE S5	S14
TABLE S6	S14
TABLE S7	S14
FIGURE S8	S15
FIGURE S9	S16
FIGURE S10	S17
FIGURE S11	S18
REFERENCES	S19

Table S1: Sequences of nucleic acids used in this study.

Oligomer	Sequence
DNA Anchor	5'-ACA CAC ACA CAC ACA CAC-3'-NH ₂
DNA Capture	5'-GTG TGT GTG TGT GTG TGT TTT CCC CCC TTT ACA TAG GTA-3'
PNA Target	^C TGT ATC CAT ^N -TAMRA
DNA Target	3'-TGT ATC CAT-5'-TAMRA
DNA-2A Target	3'-AAT GTA TCC AT-5'-TAMRA

Single Molecule Imaging Data Analysis

Images were analyzed using a super-resolution imaging scheme previously described.²⁶ First, we located all fluorescent spots in each image, and fit a 2D Gaussian to each spot to locate its centroid coordinate to high precision (~40 nm). Next, we plotted the location of all the hybridization events to determine locations that experience repeat hybridization visits by fluorescently tagged target DNA molecules to locate the probe DNA molecules. A map of the location of each surface-binding event is shown in **Figure S1**. This map is represented as a 2-D histogram, where each pixel is a 20 nm sized bin indicating the number of hybridization events at that location. Clusters of 3-30 binding events are then located, and all the events at each cluster are grouped together and ordered chronologically to define a binding “site”. The duration time and interval between each binding event defines the hybridization state of each probe molecule binding site on the surface. **Figure S2** displays examples of a single molecule trajectory showing the occupancy of a probe molecule site determined by molecule tracking (in orange), and the fluorescence intensity at that location on the surface (in blue). Note that in Figure S2, at higher ionic strength, the interval between hybridization events decreased for the 2A-DNA target and increased for the PNA target as a result of changes in the association rate. The molecule tracking result showed good agreement with the changes in fluorescence intensity as the labeled target molecules bind and unbind at that location.

For each binding site on the surface, we measured the average lifetime of each hybridization event (τ_{off}) and the average interval

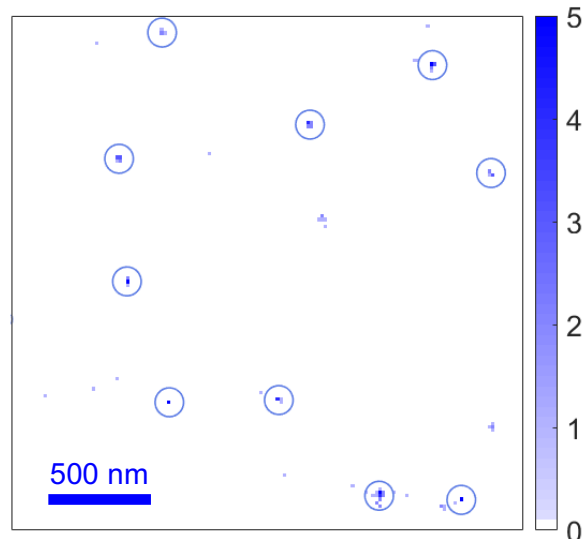


Figure S1. 2D histogram of the location of each hybridization event. The color map represents the number of events at each pixel location representing a 20 nm square bin. Circles show the locations of filtered binding sites. Data are from DNA-2A Target hybridization with probe DNA in 450 mM NaCl buffer at 22.5°C.

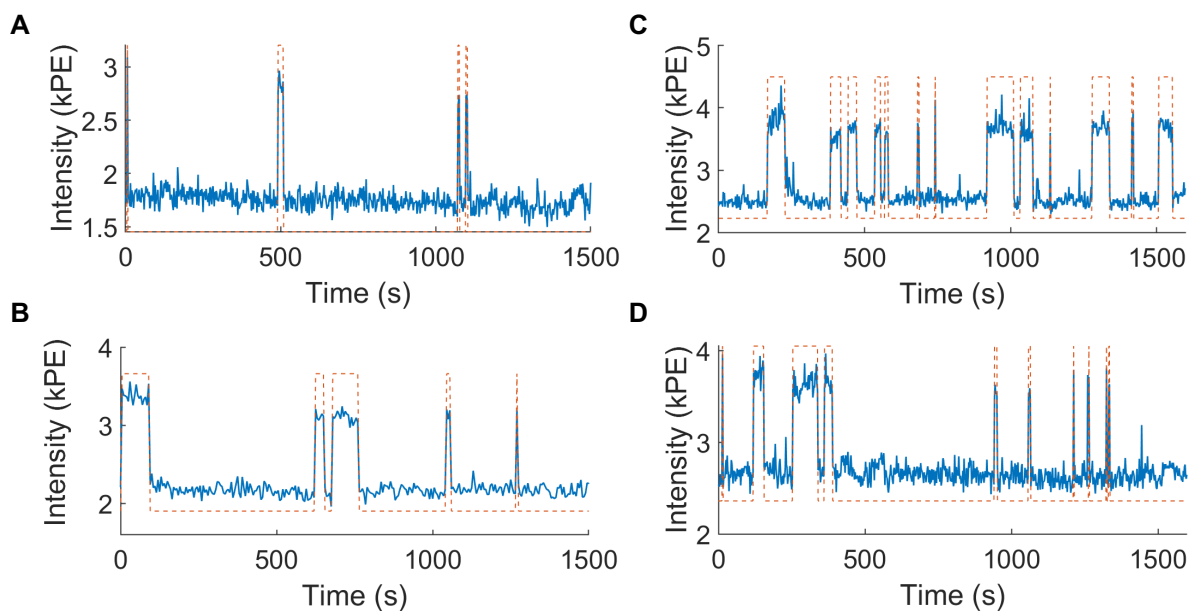


Figure S2. Single molecule trajectory for probe site showing fluorescence intensity (blue) with single molecule tracking analysis to determine site occupancy (orange line). A) Data are from DNA-2A Target hybridization with probe DNA in 100 mM NaCl buffer, and B) 450 mM NaCl. Data in C) are from the PNA Target at 100 mM NaCl, and D) 450 mM PNA Target at 450 mM NaCl. Data collected at 22.5°C.

time between hybridization events (τ_{on}). These were then used to determine the dissociation and association rate constants, respectively: $k_{off} = 1/\tau_{off}$, and $k_{on} = 1/\tau_{on}$. We filtered the molecules based on their association or dissociation rates to remove spurious nonspecific adsorption sites or photodamaged molecules. We observed that a population of probe molecules with a faster dissociation rate would appear about 20-30 minutes of exposure to laser radiation and the fluorescently labeled target. This can be seen in a 2-D histogram of the association and dissociation rate constant of each probe molecule on the surface in **Figure S3**. Other researchers have demonstrated that guanine-containing oligonucleotides are vulnerable to chemical modification by reactive oxygen species generated by the fluorescent label on the target DNA.^{1,2} Oxidation of the bases reduces the duplex stability, resulting in the formation of molecules with a faster dissociation rate constant. We believe this is happening in our system as well, as the immobilized probe has G content in the base-pairing region. To mitigate this, we limited data collection to one ~30 min data set per population of probe molecules. After collecting a data set,

the microscope stage was moved to illuminate a new population of probe molecules for the next data set. Additionally, we filtered out these photodamaged probe sites based on their dissociation kinetics. Data were only collected from the population with a slower dissociation rate, indicated by the bounding box in **Figure S3**, representing the population of probe molecules detected before significant photodamage to the probe molecule population. This is represented by the larger population in **Figure S3** with rate constants of approximately $k_{\text{off}} \sim 0.02 \text{ s}^{-1}$ and $k_{\text{on}} \sim 6 \times 10^{-3} \text{ M}^{-1} \text{ s}^{-1}$.

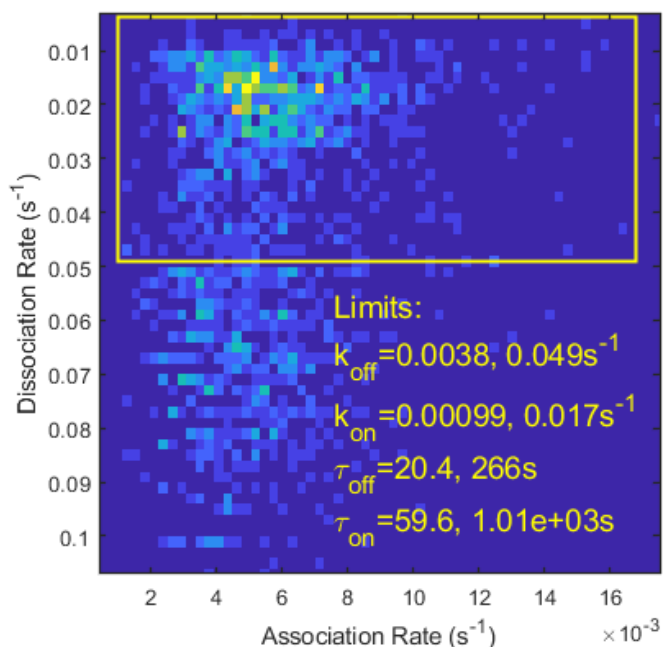


Figure S3. 2D histogram of the of the association and dissociation rate constant calculated at each binding site. Sites within the yellow bounding box are selected for analysis while photodamaged molecules with faster dissociation kinetics (lower left quadrant) are not analyzed further. Data are from DNA-2A Target hybridization with probe DNA in 450 mM NaCl buffer at 22.5 °C.

$\text{M}^{-1} \text{ s}^{-1}$. The boundaries of this box were chosen to encompass 98% of this non-photodamaged population, by fitting a Poisson-Erlang distribution to the data, and numerically integrating the fitted function to set upper and lower limits that encompass 98% of the distribution. The Poisson-Erlang function was used to describe distributions of the sum of some number of dwell times (with the number of events represented by from a Poisson distribution) selected from an exponential probability distribution. This is a good model for the process of observing a finite number of events at an individual molecule, and we have previously shown that it can be used to represent distributions of single-molecule DNA hybridization event lifetimes.³ These sites were also filtered to remove sites with other anomalies, such as events that are not interspersed throughout the video data set, and sites with an excessive number of single-frame events. This filtering process typically excludes 20-40% of binding sites across different data sets, with more sites being filtered

out on data sets with more photodamaged sites. Binding sites that meet these criteria are plotted as circles in the hybridization event map in **Figure S1**.

Hybridization event statistics were then pooled from the remaining filtered probe molecules to generate histograms of the hybridization events duration lifetimes (time-to-dissociate) and interval lifetimes (time-to-associate), as shown in **Figure S4**. These are represented as integrated cumulative histograms to better sample the tail of the exponential decay profile. Histograms were then fit to a first-order kinetics model to determine the average rate constant, k_{on} , the dissociation rate constant, k_{off} , and the association constant, K_a , $K_a = k_{on}/k_{off}$. Data in Figure S4 shows the differences in association and dissociation kinetics for the DNA-2A Target in 100 mM and 450 mM ionic strength.

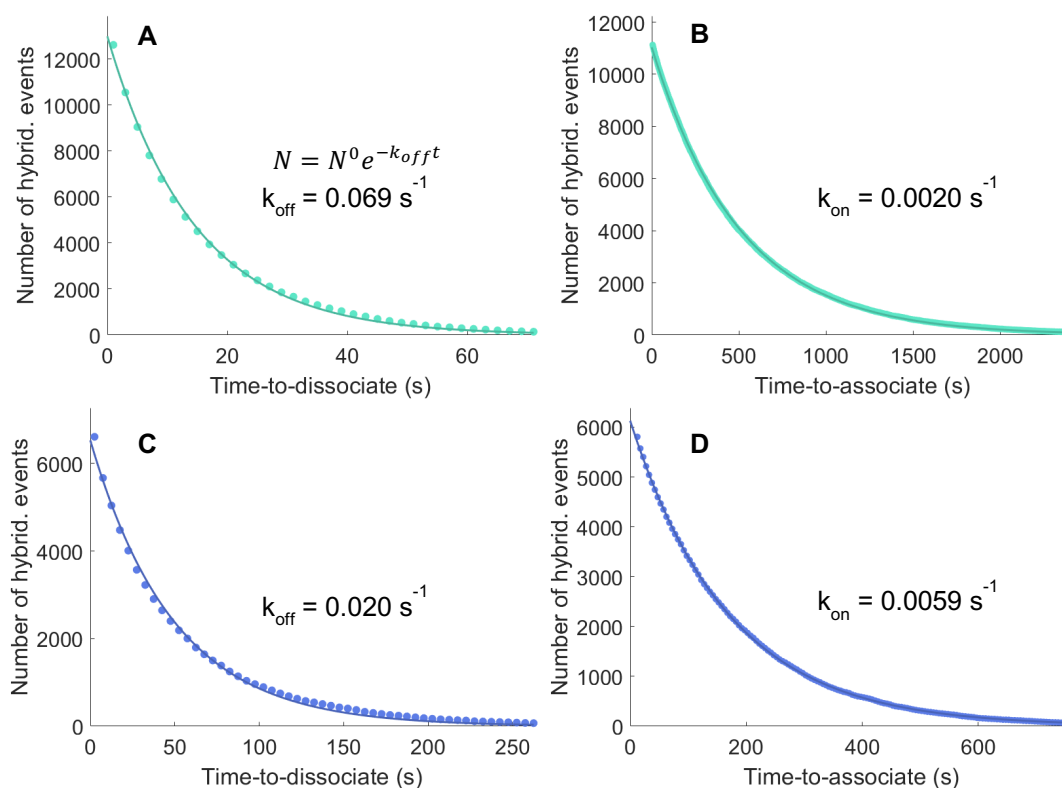


Figure S4. Cumulative histogram of association and dissociation lifetimes pooled from all probe molecules. Histograms are fit to a single exponential decay function to determine k_{on} and k_{off} respectively. Data are from DNA-2A Target hybridization with probe DNA in 100 mM NaCl Buffer showing A) time-to-dissociate histogram (k_{off}) and B) time-to-association histogram (k_{on}), and the same DNA-2A Target hybridization in 450 mM NaCl buffer showing C) k_{off} and D) k_{on} , both at 22.5 °C.

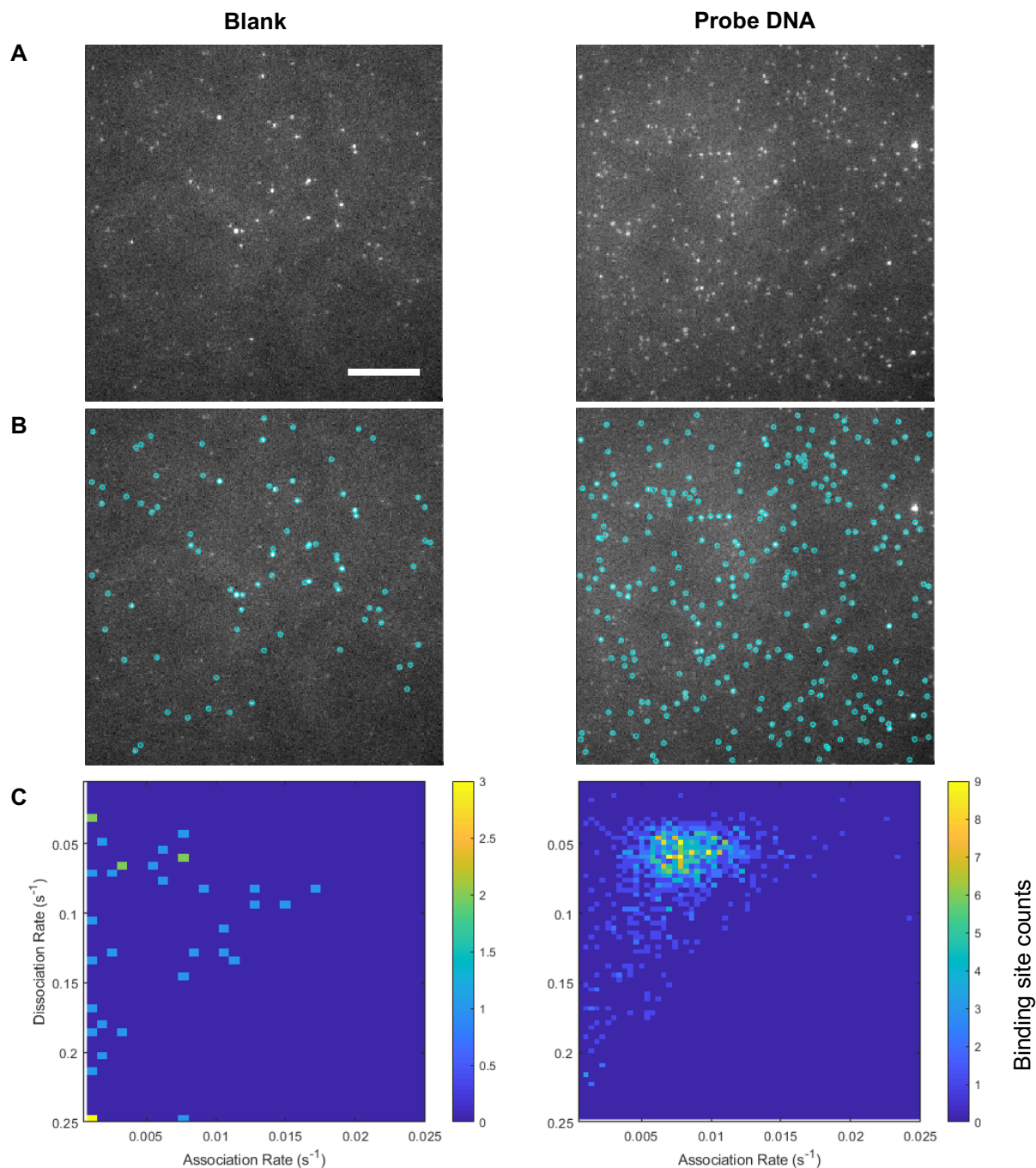


Figure S5. Comparison of blank substrate with capture sequence but no probe DNA (Left) and substrate with probe DNA immobilized at surface (Right). Solutions of 30 nM PNA target in 200 mM NaCl buffer at 27.5°C were flowed over each sample and allowed to equilibrate. (A) Example fluorescence images and (B) images with located single molecule spots shown in cyan. The data set with probe DNA had an average of 206 ± 28 molecules per image, while the blank had an average of 64 ± 14 molecules per frame. Binding sites that meet the filtering criteria described above are plotted on a 2D histogram showing the association rate and dissociation rate at each site (C). On the blank substrates, 47 sites meet the criteria. After immobilization of probe DNA, 918 sites meet the criteria, with a homogeneous cluster of sites with average dissociation rate of $0.07 s^{-1}$ and association rate of $0.008 s^{-1}$. This indicates that although nonspecific adsorption of PNA accounts for about 30% of the molecules at the interface, these nonspecific adsorption events do not repeatedly visit the same location and rarely register as binding sites using the site selection criteria. Scale bar is 10 μm .

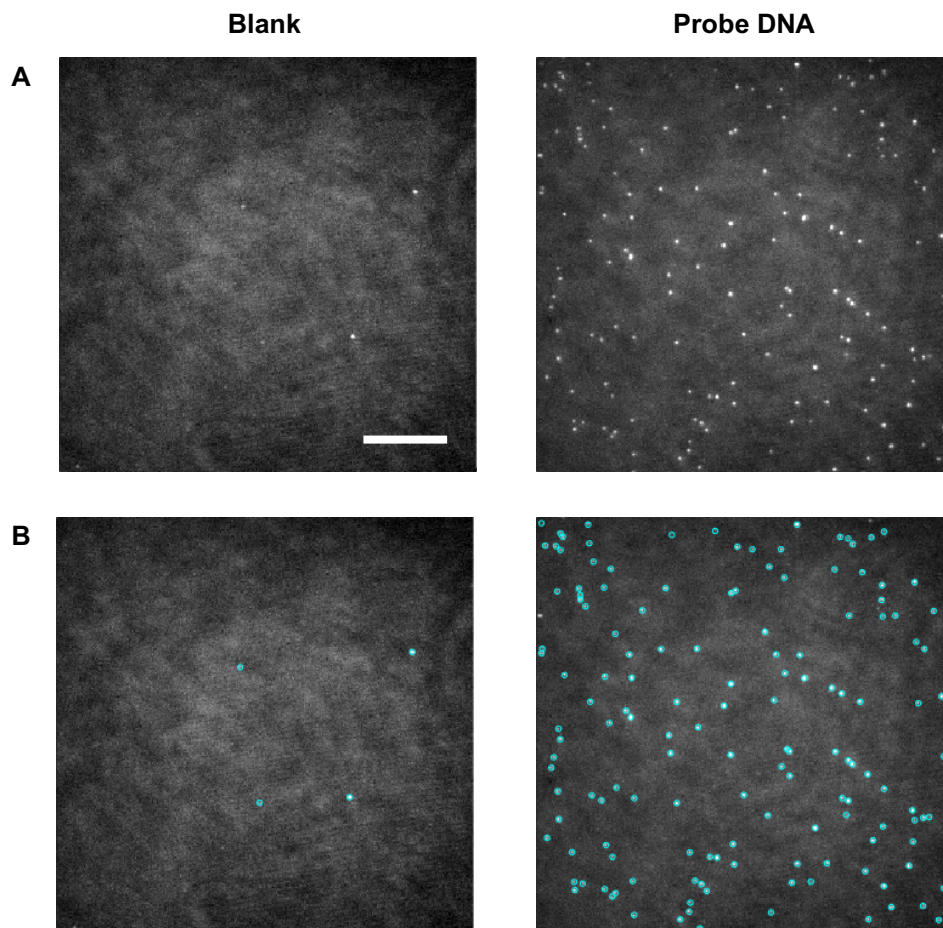


Figure S6. Comparison of blank substrate with capture sequence but no probe DNA (Left) and substrate with probe DNA immobilized at surface (Right). Solutions of 20 nM DNA-2A target in 150 mM NaCl buffer at 22.5°C were flowed over each sample and allowed to equilibrate. Example fluorescence images are shown in (A) with located single molecule spots shown in cyan (B). The data set with probe DNA had an average of 144 ± 35 molecules per image, while the blank had an average of 7 ± 3 molecules per frame. Blank data sets with DNA targets have very few apparent binding sites (for this data set none were detected).

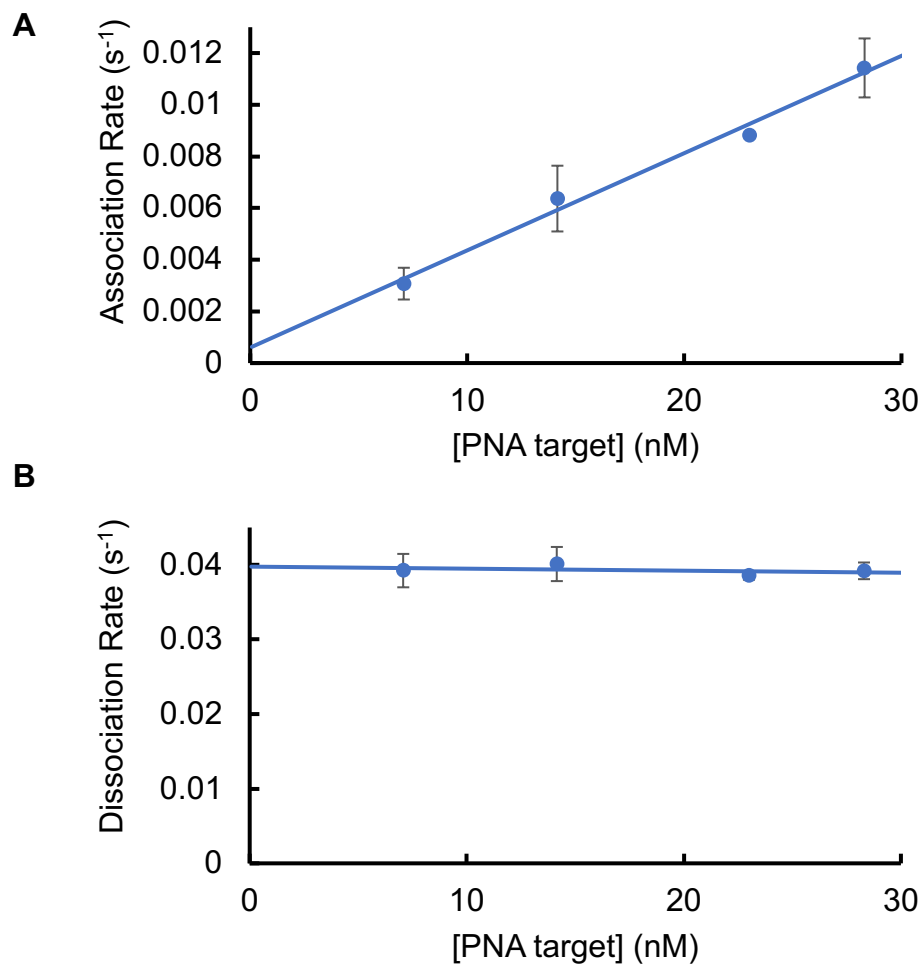


Figure S7. Trends in association and dissociation rate with varying PNA Target concentration in 200 mM NaCl and 25°C. Plot shows A) changes in measured association rate with concentration, showing an expected linear trend with slope corresponding to $k_{on} = 3.8 \pm 0.8 \text{ M}^{-1} \text{ s}^{-1}$ for this particular data set with intercept smaller in magnitude than uncertainty, and B) no significant trend in dissociation rate with changing concentration, slope is smaller in magnitude than uncertainty.

van't Hoff analysis of PNA:DNA duplex formation

In order to better understand the effect of ionic strength on the enthalpic and entropic components of PNA:DNA duplex formation, we performed a van't Hoff analysis of the calculated K_a values across the range of temperatures and salt concentrations (**Table S4**). A plot of the $\ln(K_a)$ vs the inverse of the temperature provides a relationship to determine the change in entropy (ΔH) and enthalpy (ΔS) according to **Equation S1**:

Equation S1

$$\ln K = -\frac{\Delta H}{R} \left(\frac{1}{T} \right) + \frac{\Delta S}{R}$$

The slope and intercept of the line generated from the plot were used to calculate the enthalpic and entropic changes, respectively (**Figure S8A; Table S5**). From these values, we determined the free energy (ΔG°) according to the relationship $\Delta G^\circ = \Delta H^\circ - T\Delta S^\circ$. Although the magnitude of ΔG° increased (became more negative) as ionic strength decreased (**Figure S8B**), there is no significant trend in enthalpy and entropy (**Figure S8C and S8D**). This is due to significant covariance between the slope and intercept values of the van't Hoff plots due to the narrow temperature range studied. The fitted slope and intercept have high uncertainty, making it difficult to determine enthalpy and entropy contributions across the range of ionic strength.

Transition State Energies of Duplex Formation

We next sought to determine the energy differences between the single-stranded oligos or PNA:DNA duplex compared to the transition states for association or dissociation using Eyring transition state theory.⁴ The Eyring equation (**Equation S2**) describes the relationship between the kinetic rate constant, k , and the free energy, ΔG^\ddagger , of the transition state (TS) based on the transmission coefficient κ , Boltzmann's constant, k_B , and Planck's constant, h .

Equation S2

$$k = \frac{\kappa k_B T}{h} e^{-\frac{\Delta G^\ddagger}{RT}}$$

Using the relation $\Delta G^\ddagger = \Delta H^\ddagger - T\Delta S^\ddagger$, we can derive the linearized Eyring equation (**Equation S3**) and use it to determine the transition state thermodynamics from the association and dissociation rate constants by plotting the $\ln(k/T)$ vs $1/T$ and fitting a linear regression (**Figure S9A and S9A; Table S4 and S5**).

Equation S3

$$\ln \frac{k}{T} = \frac{-\Delta H^\ddagger}{R} \frac{1}{T} + \ln \frac{k_B}{h} + \frac{\Delta S^\ddagger}{R}$$

The slope of the regression line was used to calculate the change in enthalpy. To calculate the change in entropy of the TS, we estimated the transmission coefficient to be 1, where the complex at the TS is equally likely to form a duplex or single strand. We estimate the maximum duplex formation attempt frequency to be the ratio of Boltzmann's constant, k_B , to Planck's constant, h . We see that ΔG^\ddagger between single strands and TS decreased at lower ionic strengths, suggesting a lower barrier to formation of the TS at lower ionic strength (**Table S6; Figure S9B**). Conversely, the change in ΔG^\ddagger between the PNA:DNA duplex and TS was minimal with a slight increase at lower ionic strength (**Table S7; Figure S10B**). However, we again observed large uncertainties in ΔH^\ddagger and ΔS^\ddagger . While the trends for both single strands and duplex to TS appear positive with increasing ionic strength for both ΔH^\ddagger and ΔS^\ddagger , the magnitude of the changes were not significant enough to accurately conclude how ionic strength affects this response (**Figure S9C and S9D; Figure S10C and S10D**). This is due to both measurement uncertainty in the rates, and the small changes in rate over the relatively small temperature range studied. Future work will be needed to measure PNA:DNA duplex formation and dissociation rates over a wider temperature range in order to better understand how the change in enthalpy and entropy of the transition state are affected by ionic strength.

The Eyring plots in **Figures S8A and S9A** were also used to estimate the best-fit values and uncertainties of the kinetic rate constants and association constants of PNA:DNA duplex

formation at 22.5°C shown in **Figure 4** and **Figure 5**. These rates were determined from the predicted y-value from the linear regression fit (corresponding to $\ln(k_{\text{off}}/T)$ or $\ln(k_{\text{on}}/T)$) with uncertainty from the standard error of the predicted y-value.⁵ Because the standard error from the plot is in natural log units, the upper and lower uncertainty bounds of the rate constants on a linear scale are not equal in size. To simplify reporting, we represent the uncertainties in figures as the average deviation of the upper and lower bounds from the predicted rate constant.

Table S2: Values of DNA:DNA hybridization kinetics parameters determined from single-molecule hybridization events pooled from all probe sites at 22.5°C. Uncertainties are 2 standard deviations of the mean calculated from 3 repeat measurements.

[NaCl] (mM)	k_{off} (s^{-1})	k_{on} ($\mu\text{M}^{-1}\text{s}^{-1}$)	K_{a} (μM^{-1})
450	0.34 ± 0.05	0.44 ± 0.09	1.3 ± 0.4

Table S3: Values of DNA-2A:DNA hybridization kinetics parameters determined from single-molecule hybridization events pooled from all probe sites at 22.5°C. Uncertainties are 2 standard deviations of the mean. *Data at 50 mM were from a single measurement, uncertainties are estimated from the average relative standard deviation measured at 100-450 mM NaCl.

[NaCl] (mM)	k_{off} (s^{-1})	k_{on} ($\mu\text{M}^{-1}\text{s}^{-1}$)	K_{a} (μM^{-1})
50*	$0.08 \pm 0.01^*$	$0.031 \pm 0.005^*$	$0.37 \pm 0.07^*$
100	0.063 ± 0.006	0.06 ± 0.01	1.02 ± 0.09
150	0.045 ± 0.002	0.09 ± 0.01	2.1 ± 0.2
200	0.033 ± 0.003	0.12 ± 0.02	3.8 ± 0.9
300	0.0234 ± 0.0008	0.158 ± 0.002	6.7 ± 0.1
450	0.021 ± 0.002	0.19 ± 0.01	9.2 ± 0.6

Table S4: Values of PNA:DNA hybridization kinetics parameters determined from single-molecule hybridization events pooled from all probe sites.

Temperature (°C)	[NaCl] (mM)	k_{off} (s^{-1})	k_{on} ($\mu\text{M}^{-1} \text{s}^{-1}$)	K_a (μM^{-1})
22.5	50	0.021	0.40	19
	100	0.019	0.30	16
	150	0.020	0.23	11
	200	0.020	0.18	9.2
	300	0.024	0.16	6.5
	450	0.027	0.12	4.3
25	50	0.031	0.59	19
	100	0.029	0.41	14
	150	0.039	0.30	7.7
	200	0.035	0.27	7.6
	300	0.042	0.19	4.5
	450	0.044	0.18	4.1
27.5	50	0.051	0.60	12
	100	0.058	0.43	7.5
	150	0.059	0.37	6.1
	200	0.065	0.29	4.5
	300	0.071	0.24	3.3
	450	0.081	0.17	2.1
30	50	0.11	0.72	6.4
	100	0.15	0.58	3.8
	150	0.16	0.42	2.7
	300	0.20	0.30	1.5
	450	0.20	0.27	1.3

Table S5: Thermodynamic values of PNA:DNA hybridization determined by van't Hoff analysis. Uncertainty of ΔH and ΔS are 1 standard error from the van't Hoff plot uncertainty in slope and intercept. Uncertainty in ΔG is determined from the uncertainty in the predicted y-value in the van't Hoff plot.

[NaCl] (mM)	ΔH (kJ mol ⁻¹)	ΔS (J K ⁻¹ mol ⁻¹)	ΔG at 22.5°C (kJ mol ⁻¹)
50	-110 ± 30	-200 ± 100	-41.7 ± 0.7
100	-150 ± 30	-400 ± 100	-41.1 ± 0.7
150	-130 ± 30	-320 ± 90	-40.1 ± 0.7
200	-100 ± 30	-220 ± 90	-39.6 ± 0.5
300	-140 ± 20	-340 ± 70	-38.8 ± 0.6
450	-130 ± 20	-300 ± 80	-37.9 ± 0.6

Table S6: Thermodynamic values of the changes from ground state single strands to transition state determined by Eyring plots of $\ln(k_{off}/T)$ and $1/T$. Uncertainty of ΔH^\ddagger and ΔS^\ddagger are 1 standard error from the Eyring plot uncertainty in slope and intercept. Uncertainty in ΔG^\ddagger is determined from the uncertainty in the predicted y-value in the Eyring plot.

[NaCl] (mM)	ΔH^\ddagger (kJ mol ⁻¹)	ΔS^\ddagger (J K ⁻¹ mol ⁻¹)	ΔG^\ddagger at 22.5°C (kJ mol ⁻¹)
50	-60 ± 10	50 ± 40	40.5 ± 0.4
100	-62 ± 7	70 ± 20	41.3 ± 0.2
150	-58 ± 7	60 ± 20	41.9 ± 0.1
200	-80 ± 20	120 ± 60	42.5 ± 0.4
300	-67 ± 6	80 ± 20	43.0 ± 0.1
450	-80 ± 20	120 ± 60	43.6 ± 0.5

Table S7: Thermodynamic values of the changes from ground state duplex to transition state determined by Eyring plots of $\ln(k_{off}/T)$ and $1/T$. Uncertainty of ΔH^\ddagger and ΔS^\ddagger are 1 standard error from the Eyring plot uncertainty in slope and intercept. Uncertainty in ΔG^\ddagger is determined from the uncertainty in the predicted y-value in the Eyring plot.

[NaCl] (mM)	ΔH^\ddagger (kJ mol ⁻¹)	ΔS^\ddagger (J K ⁻¹ mol ⁻¹)	ΔG^\ddagger at 22.5°C (kJ mol ⁻¹)
50	-170 ± 20	310 ± 70	82.1 ± 0.5
100	-220 ± 30	500 ± 100	82.5 ± 0.7
150	-210 ± 20	420 ± 60	82.1 ± 0.5
200	-190 ± 30	370 ± 80	82.0 ± 0.5
300	-220 ± 20	460 ± 80	81.8 ± 0.6
450	-210 ± 20	420 ± 80	81.5 ± 0.5

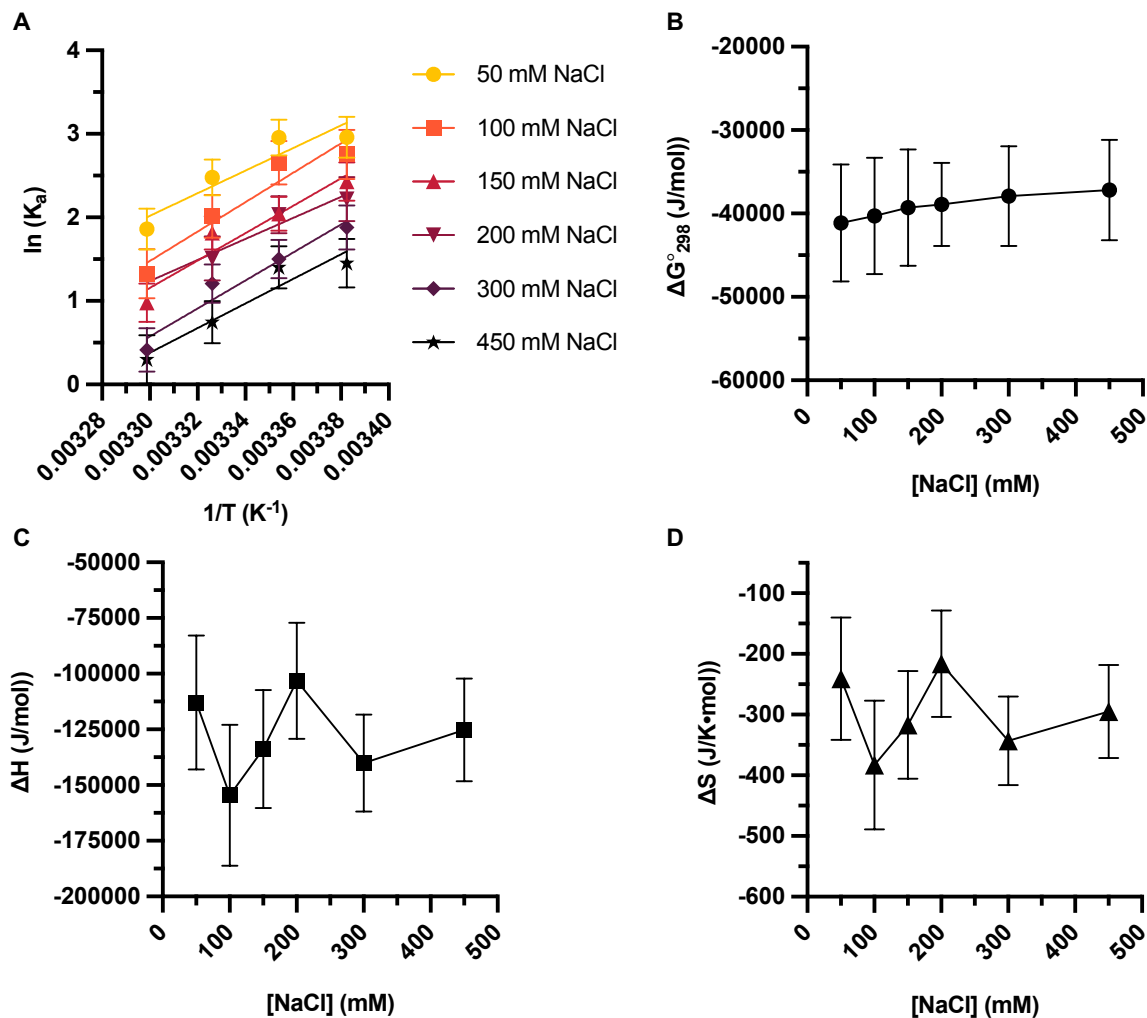


Figure S8: Thermodynamic changes in relationship to ionic strength. A) van't Hoff plot showing the linear relationship between $\ln(K_a)$ and $1/T$. Changes in B) free energy (ΔG), C) enthalpy (ΔH), and D) entropy (ΔS) across ionic strengths. While a positive trend is observed for ΔG , no observable trend is present for ΔH or ΔS .

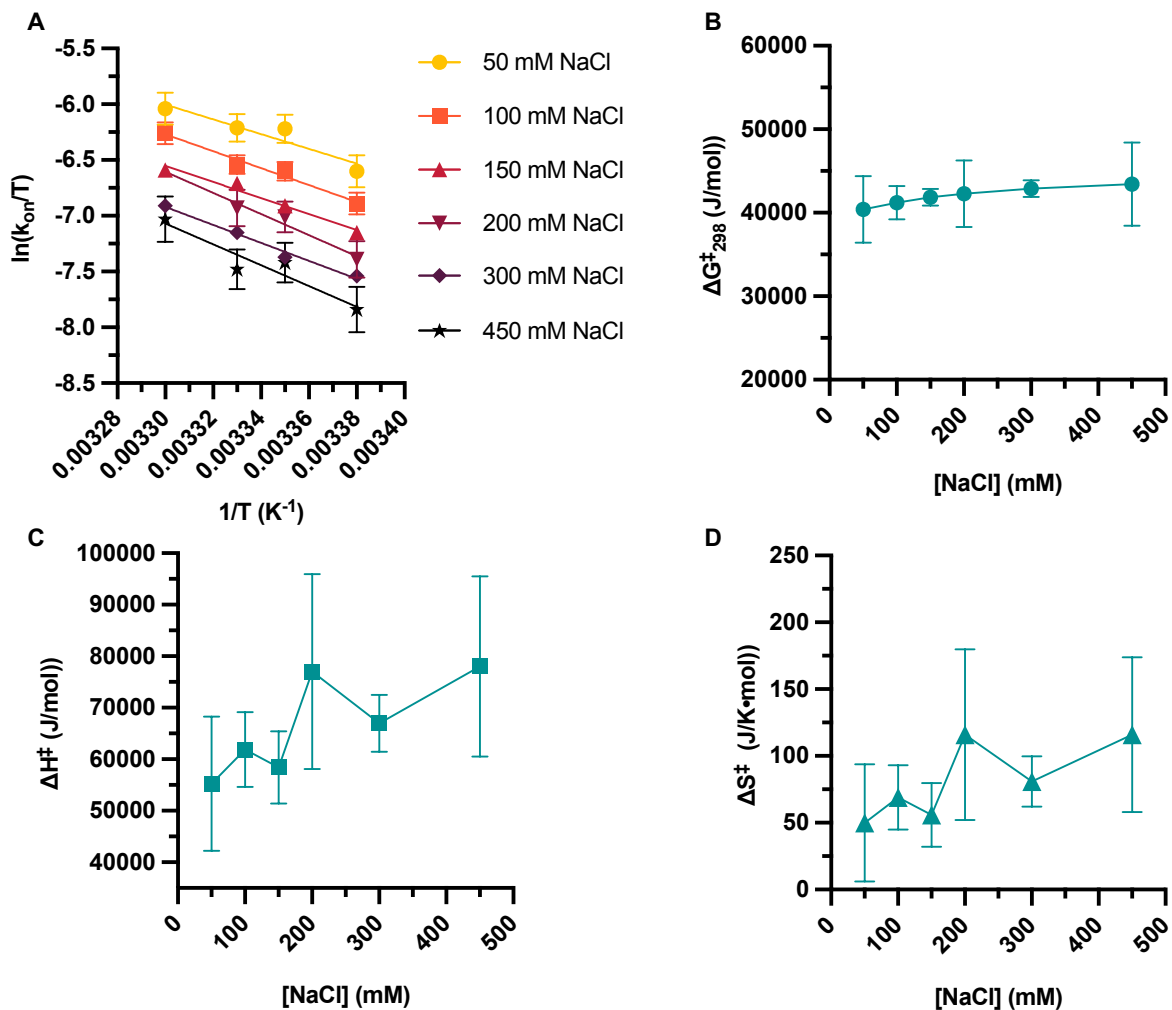


Figure S9: Thermodynamic changes between ground state single strands and transition state in relationship to ionic strength. A) Eyring plot showing the linear relationship between $\ln(k_{\text{on}}/T)$ and $1/T$. Changes in B) free energy (ΔG^{\ddagger}), C) enthalpy (ΔH^{\ddagger}), and D) entropy (ΔS^{\ddagger}) from the ground state single strands to the transition state across ionic strength.

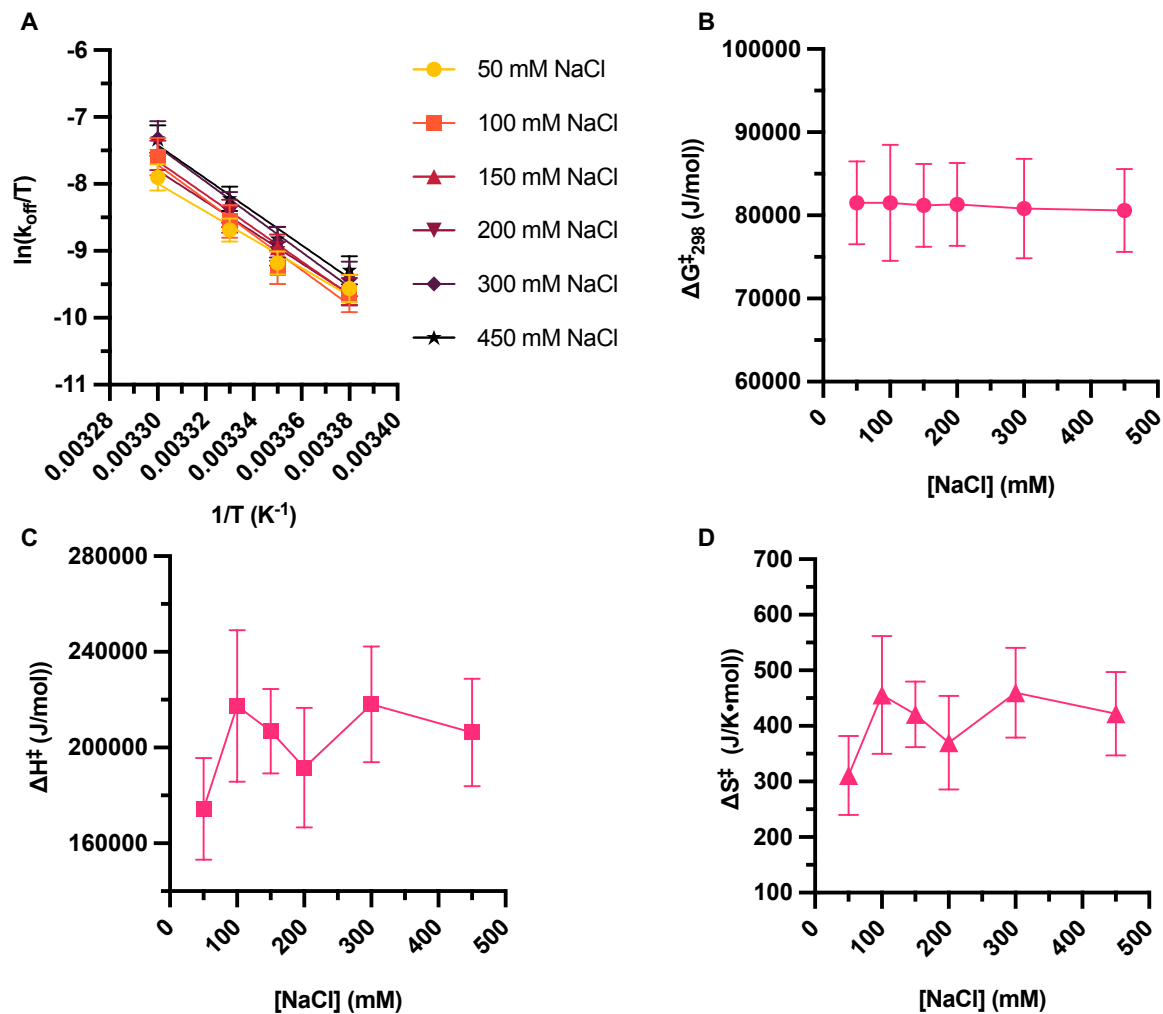
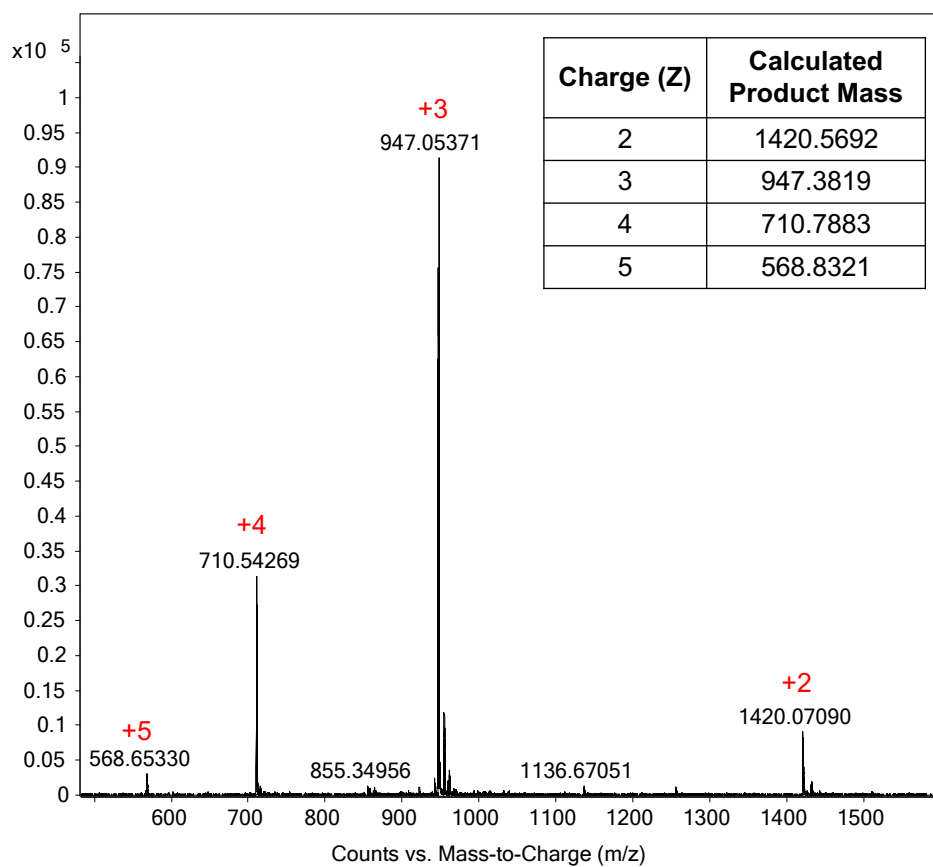
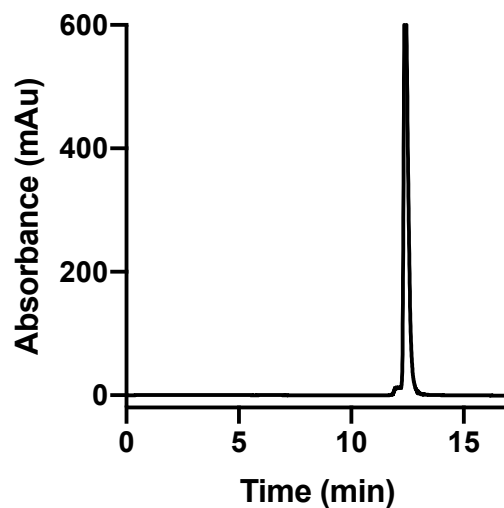
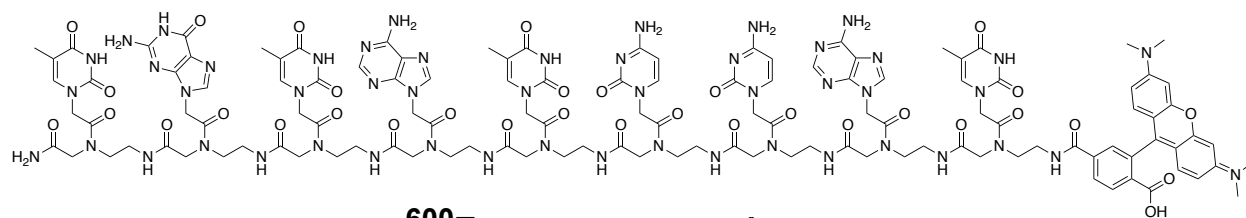


Figure S10: Thermodynamic changes between ground state duplex and transition state in relationship to ionic strength. A) Eyring plot showing the linear relationship between $\ln(k_{off}/T)$ and $1/T$. Changes in B) free energy (ΔG^{\ddagger}), C) enthalpy (ΔH^{\ddagger}), and D) entropy (ΔS^{\ddagger}) from the ground state duplex to the transition state across ionic strength.

Figure S11. Top: Structure of peptide nucleic acid oligomer “PNA Target”, Middle: HPLC chromatogram of PNA target measured as described in the Experimental Section, Bottom: ESI-TOF mass spectrum of pure oligomer and table of calculated (expected) mass at each charge state.



References:

1. P. Blumhardt, J. Stein, J. Mücksch, F. Stehr, J. Bauer, R. Jungmann and P. Schwille, *Molecules*, 2018, **23**, 3165.
2. J. Sobek, M. Schmidt, J. Grossmann, H. Rehrauer, L. Schmidt and R. Schlapbach, *Methods Appl. Fluoresc.*, 2020, **8**.
3. E. M. Peterson and J. M. Harris, *Anal. Chem.*, 2018, **90**, 5007-5014.
4. H. Eyring, *J. Chem. Phys.*, 1935, **3**, 107-115.
5. D. C. Montgomery, *Applied statistics and probability for engineers*, Wiley, New York, 2003.